Global minima of transition metal clusters described by Finnis-Sinclair potentials: a comparison with semi-empirical molecular orbital theory

James Elliott, Yasushi Shibuta, David Wales

Global minima of transition metal clusters described by Finnis-Sinclair potentials: a comparison with semi-empirical molecular orbital theory

Journal:	*Philosophical Magazine & Philosophical Magazine Letters*
Manuscript ID:	TPHM-09-May-0230.R1
Journal Selection:	Philosophical Magazine
Date Submitted by the Author:	18-Aug-2009
Complete List of Authors:	Elliott, James; University of Cambridge, Materials Science and Metallurgy Shibuta, Yasushi; University of Tokyo, Materials Engineering Wales, David; University of Cambridge, Chemistry
Keywords:	Monte-Carlo, nanosized clusters, numerical simulation, transition metals
Keywords (user supplied):	Finnis-Sinclair potential, global optimization, semi-empirical orbital theory

Philosophical Magazine
Vol. 00, No. 00, 2009, 1–17

RESEARCH ARTICLE

Global minima of transition metal clusters described by Finnis–Sinclair potentials: a comparison with semi-empirical molecular orbital theory

J. A. Elliott[a*], Y. Shibuta[b] and D. J. Wales[c]

[a]*Department of Materials Science and Metallurgy, University of Cambridge, Pembroke Street, Cambridge, CB2 3QZ, UK*; [b]*Department of Materials Engineering, The University of Tokyo, 7-3-1 Hongo, Bunkyo-ku, Tokyo 113-8656, Japan*; [c]*Department of Chemistry, University of Cambridge, Lensfield Road, Cambridge, CB2 1EW, UK.*

(*v4.0, 18 August 2009*)

We present putative global minimum energy structures for nanoscopic transition metal clusters, with sizes ranging from $N = 3$ to 100 atoms, described by the original embedded atom potential of Finnis and Sinclair (FS) [1], using their parameter sets for molybdenum [1] and iron [2], and compare selected results with predictions from semi-empirical molecular orbital (SE-MO) theory via further optimization using the AM1* [3] and PM6 [4] Hamiltonians. We find that, for Fe clusters, the global minima found for FS potential consist mainly of polyicosahedral structures with magic numbers $N = 13, 19, 23, 26, 29, 39, 60$ and 78, whereas, for Mo clusters with sizes $N > 30$, they are more likely to be bcc terminated by {110} and {100}-type surface facets. We find that the global minimum energy structures obtained for the FS potential are, in general, very good starting points for further SE-MO optimization, although the relative ordering of the resulting structures by energy compared to those obtained from global minima of other potentials used to model metal clusters does not in general agree.

Keywords: Finnis–Sinclair potential, transition metal, nanosized clusters, numerical simulation, global optimization, basin-hopping, semi-empirical molecular orbital theory, AM1*, PM6

1. Introduction

The structures of transition metal nanoclusters (with diameters between 1 and 10 nm) are of significant theoretical and practical interest due to their potential use in ultra-high density magnetic recording materials [5], catalytic particles in the synthesis of carbon nanotubes [6–9], and other applications in electronics and optics. Due to their small size, nanoclusters can remain in a 'liquid-like' state at temperatures well below the bulk melting point [10–12], and their magnetic moments can exceed bulk values up to cluster sizes of several hundred atoms [13]. In general, the geometric structures of the clusters do not resemble those of the bulk metals since there are no constraints on rotational symmetry from the crystallographic restriction theorem. Instead, stable clusters with sizes corresponding to 'magic numbers' of aperiodic motifs (e.g. icosahedra, decahedra and tetrahedra) are commonly observed. While there exists much previous work on global optimization of metal clusters described by a variety of different potentials, which

*Corresponding author. Email: jae1001@cam.ac.uk

ISSN: print/ISSN online

DOI:
http://www.informaworld.com

is briefly reviewed in section 1.1, to date there has been no systematic study of clusters described by Finnis–Sinclair (FS) potentials, as originally proposed for bcc metals, such as iron and molybdenum. In view of the current widespread use of these potentials to describe transition metal clusters, we have therefore undertaken such an investigation to mark the 25th anniversary of the first publication of the FS potential.

1.1. *Global optimization of metal clusters*

The number of distinct structures (disregarding permutational isomers) corresponding to local minima on the potential energy surface (PES) of a cluster containing N atoms is expected to grow exponentially with N [14, 15]. Systematic global optimization techniques are therefore essential to identify favourable morphologies [16]. In fact, the computational expense of locating the global minimum with some degree of confidence is not a monotonic function of N, even for values of N much larger than those considered in the present work. At sizes where there is a single favourable morphology, the potential energy landscape corresponds to a single funnel topology. Such landscapes correspond to good 'structure-seekers', where global optimization is generally a straightforward task [17]. In contrast, numerous cases have been found where the landscape exhibits two or more potential energy funnels corresponding to competing morphologies. If the global potential energy minimum is entropically disfavoured then such systems exhibit low temperature solid-solid transitions between different phase-like forms, associated with different regions of configuration space [18–22]. Global optimization is generally much more difficult in this situation [16, 22–24].

The basin-hopping approach to global optimization is based upon large steps in configuration space between local minima [23], generalizing the 'Monte Carlo plus energy minimization' procedure of Li and Scheraga [25]. A key feature of the method is that a local minimization is performed after every proposed step, and that steps are accepted or rejected based upon the potential energy (and perhaps other properties) of the new minimum and the previous one in the sequence. The local minimization was recognized [16, 23] as an essential step on examination of previous studies for clusters bound by the Lennard–Jones (LJ) potential, including genetic algorithms [26, 27]. The minimization has been compared to Lamarckian rather than Darwinian evolution [28], where parents pass on features that they have acquired, rather than inherited, to their 'offspring'.

Perhaps the most attractive feature of the basin-hopping approach is that only a small number of adjustable parameters need to be specified to produce acceptable results for a wide range of different systems, ranging from atomic and molecular clusters [16, 22, 23, 29, 30] to peptides [31–37], polymers [38], a glass-forming solid [39], and mesoscopic building blocks that form shells and helices [40, 41]. The `GMIN` program [42], available for use under the GNU General Public License, contains a wide variety of different step-taking approaches, along with parallel basin-hopping implementations and taboo lists [43]. The Cambridge Cluster Database [44] (CCD) serves as a repository for global optimization results, and includes energies and structures for a wide variety of model metal clusters. The structural data has proved to be particularly useful for comparisons with experimental observables, such as 'magic numbers' and diffraction patterns [45]. For atomic clusters bound by a new potential, a very efficient strategy for identifying likely global minima is simply to relax the known low-lying structures obtained in systematic studies of other systems. Here, the databases obtained for different parameterizations of the Sutton–Chen (SC) potential [46] and for the Morse potential

as a function of the range parameter are particularly useful [24, 47]. The other entries for metal clusters in the CCD include data for sodium [48] (Gupta [49, 50] and Murrell–Mottram (MM) [51–53] potentials), aluminimum [54] (glue potential [55]), lead [45, 56] (glue [57] and Gupta [49, 50] potentials), and noble metals [58], along with more systematic results for the Gupta potential [59, 60].

Recent successes for structure prediction include a combination of theory and experiment to characterize gold clusters [61]. Systematic global optimization studies such as this are likely to play an increasing role in future work, especially for the added complexities associated with bimetallic clusters [62–64] (nanoalloys) and the use of non-metal additives, such as sulphur, which is known to enhance the yield and purity of carbon nanotubes grown by chemical vapour deposition using iron nanoparticles as a catalyst [65]. As a first step, an investigation of the PES of clusters bound by the FS potential using basin-hopping is required. We begin by briefly reviewing the properties of this potential, and its previous application to transition metal clusters.

1.2. *Application of the FS potential to transition metal clusters*

The FS potential interaction is defined, for an ensemble of N atoms with separations r_{ij}, by equation (1):

$$E = \frac{1}{2}\sum_{i=1}^{N}\sum_{j=1}^{N} V_{ij}(r_{ij}) - A\sum_{i=1}^{N}\sqrt{\rho_i} \tag{1}$$

where the total electronic charge at the site of atom i is:

$$\rho_i = \sum_{j=1,i\neq j}^{N} \phi_{ij}(r_{ij}) \tag{2}$$

$$\text{and} \qquad V_{ij}(r_{ij}) = \begin{cases} (r_{ij}-c)^2\left(c_0 + c_1 r_{ij} + c_2 r_{ij}^2\right), & r \leq c, \\ 0, & r > c, \end{cases} \tag{3}$$

is a repulsive two-body interaction, interpreted in the context of tight-binding theory as the repulsion between core electrons on neighbouring atoms, and:

$$\phi_{ij}(r_{ij}) = \begin{cases} (r_{ij}-d)^2 + \beta\frac{(r_{ij}-d)^3}{d}, & r \leq d, \\ 0, & r > d, \end{cases} \tag{4}$$

is a cohesive term related to the sum of squares of overlap integrals for the valance electrons. For each atom (or atom pair), there are seven variable parameters determined empirically by Finnis and Sinclair for bcc metals: A is the binding energy, c_0, c_1, and c_2 are free parameters used for fitting to experimental data, c and d are cut-off parameters assumed to lie between the second-nearest- and third-nearest-neighbour atoms, and β is a parameter used to introduce a maximum value of ϕ within the first-nearest-neighbour distance. This parameter is used to reproduce the anomalously low value of the Cauchy pressure, which is a function of ϕ, for iron and chromium.

Table 1. Parameters of the FS potential for iron and molybdenum, determined by Finnis and Sinclair [1, 2].

Parameter	d [Å]	A [eV]	β	c [Å]	c_0	c_1	c_2
Iron	3.569745	1.828905	1.8	3.40	1.2371147	−0.3592185	−0.0385607
Molybdenum	4.114825	1.887117	0	3.25	43.4475218	−31.9332978	6.084249

Table 2. Properties of bulk bcc Fe (lattice parameter, binding energy, bulk moduli and three elastic constants) calculated with FS potential used in this study in comparison with experimental data and ab initio calculations using DFT.

Property	a_0 [Å]	E_0 [eV/atom]	K [GPa]	c_{11} [GPa]	c_{12} [GPa]	c_{44} [GPa]
Finnis–Sinclair	2.8665	−4.28	173.1	243.1	138.1	121.9
Experiment [66, 67]	2.8665	−4.28	178.3	242.0	146.5	112.0
Ab initio (DFT) [68]	2.84	−4.28	186.0	279.0	140.0	99.0

The form of the repulsive two-body interaction [equation (3)] and cohesive term [equation (4)] as a function of atomic separation are shown in Figure 1 for the parameters given by Finnis and Sinclair for molybdenum [1] and iron (revised in Ref. [2]), which are reproduced for reference in Table 1. In the case of iron, a maximum in ϕ is observed at $r_{ij} = 2.25\,\text{Å}$, which is within the first-nearest-neighbour distance, 2.49 Å. This difference has some significant consequences for the type of clusters produced by basin-hopping (see Section 2.1) and also the ease of finding the global minimum structure. In order to introduce this maximum for both Fe and Cr, which is required to reproduce their anomalously low Cauchy pressures, equation (4) contains a cubic correction term that may give rise to incorrect behaviour at small r. In most normal applications of the potential, such small values of r do not arise, but during basin-hopping the searches described in Section 2.1, when $\beta > 0$, it was necessary to restrict $r_{ij} \geq d(\beta - 1)/\beta$ in equation (4) to avoid ϕ becoming negative and hence resulting in an undefined energy in equation (1).

The FS potential is one of the most commonly used interatomic potentials for bcc metals, since it can correctly reproduce their bulk material properties despite its empirical form and short cut-off distance. A comparison of the lattice parameters, binding energies, bulk moduli and selected elastic constants calculated for bulk bcc Fe using FS potential with equivalent experimental and ab initio results is shown in Table 2. However, for fcc metals, the alternative long-range form of the FS potential due to Sutton and Chen [46] is more widely used.

Although the FS potential was originally fitted to the material properties of bulk bcc systems, in which the coordination number is generally higher than that of a small cluster, the FS potential was applied by Marville and Andreoni [69] to examine the size-dependence of the structural properties of transition metal clusters. They showed that the dodecahedral structure, which is a type of bcc cluster, is more stable than cuboctahedral and icosahedral structures in clusters up to 3000 atoms in size. However, their calculations mainly assumed a fixed structure for the cluster, with only the 'lattice constant' allowed to relax as a function of size. More recently, Shibuta and Suzuki [70] carried out explicit molecular dynamics simulations of the phase transition from liquid droplet to solid nanoparticle for clusters, ranging in size from 2000 to 31250 atoms for iron, chromium, molybdenum, and tungsten described by FS potentials. These simulations confirmed that only nanoparticles with a bcc structure were observed, independent of particle size and elemental composition.

On the other hand, Besley et al. [71] examined the transition between fcc and bcc structures as the most stable form for an iron cluster using a Murrell–Mottram

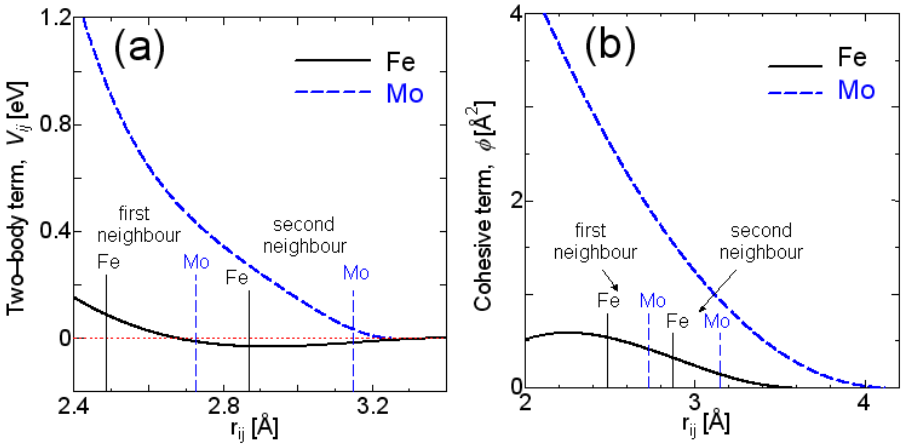

Figure 1. (a) Two-body core-core repulsion energy [equation (3)], and (b) many-body cohesive term [equation (4)] for iron and molybdenum as a function of atomic separation. The first- and second-nearest neighbour distances are indicated in each figure.

(MM) potential and found the stability order: icosahedral > rhombic dodecahedral (bcc) > decahedral > cuboctahedral (fcc) for clusters with fewer than 2000 atoms. Furthermore, Tománek et al. [72] examined the structural stability of small bcc clusters by formulation of the cohesive energy, including surface energy, and found that fcc clusters are more stable below some critical size: for example, 580 atoms for chromium. In view of these previous studies, and the considerable uncertainty that still remains in determining the most stable structures for transition metal nanoclusters, a systematic search of the global minima of small clusters described by the FS potential is desirable. Furthermore, since the FS potential cannot explicitly take into account interactions between atomic and electronic degrees of freedom in the clusters, a comparison with structures calculated using semi-empirical molecular orbital theory has been performed. A brief summary of the latter is given in following section, and the reader is referred to [4, 73, 74], and references therein, for a fuller discussion of the approximations involved.

1.3. *Semi-empirical molecular orbital (SE-MO) theory*

Until relatively recently, semi-empirical molecular orbital (SE-MO) methods based on the neglect of diatomic differential overlap (NDDO) approximation, such as AM1 [75], were restricted to main group elements containing only s and p electrons. However, Voityuk and co-workers first described an extension of AM1 to d orbitals, which they called AM1/d, and recently reported parameters for Mo [76]. Their approach was based on an extended multipole-multipole interaction scheme [77] and the introduction of two bond-specific parameters for Mo into the core-core repulsion term [76]. The Mo parameters in AM1/d were later incorporated in a slightly modified form by the Clark group into their AM1* Hamiltonian [3], which used a distance-dependent core-core repulsion for some interactions. More recently, Stewart [4] has published parameter sets for 70 elements, known as PM6 and including the transition metals Fe, Co, Ni and Mo, which use a very similar core repulsion function to AM1/d and AM1*, given by:

$$E_n = Z_A Z_B \langle s_A s_A \mid s_B s_B \rangle \left\{ 1 + \delta_{AB} \exp\left[-\alpha_{AB} \left(R_{AB} + 0.0003 R_{AB}^6 \right) \right] \right\} \qquad (5)$$

where $Z_{A/B}$ are the atomic numbers, R_{AB} is the separation, and $\langle s_A s_A \mid s_B s_B \rangle$ are

the two-electron, two-centre integrals between species A and B. The bond-specific parameters δ_{AB} and α_{AB} were determined by fitting to experimental enthalpies of formation and geometries for selected molecules [4], and determine the range of the repulsions between core electrons in an analogous way to equation (3) for the FS potential. For transition metals, the bonding character of the interactions is provided by the overlap of d electrons in the valence band.

Thus, in principle, the empirical form of the FS potential should be compatible with the description of electronic bonding in SE-MO methods such as AM1* and PM6, or alternatively density-functional based tight binding (DFTB) approaches [78]. However, the advantages of SE-MO methods are that they give a self-consistent calculation of the ground-state energy and an explicit representation of the electronic wave function and spin density without the computational expense of a full density functional theory (DFT) calculation. Also, due to the way in which they are parameterized, as opposed to an exact Hartree-Fock (HF) approach, SE-MO Hamiltonians implicitly include the effects of electron correlation [79], which is required to describe phenomena such as ferromagnetism [80]. However, without performing a full configuration interaction (CI) calculation, which is prohibitive for even modestly sized systems, it is difficult to determine the precise electronic ground state and, for open-shell unrestricted calculations without projection, there is a risk of spin contamination from excited states. For these reasons, we have not attempted here a detailed comparison of the magnetic moments predicted for different clusters by SE-MO methods. However, in Section 3.2, some of the global minimum cluster structures calculated using FS potentials are compared with those obtained after further optimization using SE-MO theory, in an attempt to isolate the structural changes caused by the inclusion of exchange-correlation energy.

2. Methodology

2.1. *Global optimization*

All the global optimization calculations in the present work were carried out using the `GMIN` package [42], which implements the basin-hopping algorithm with a variety of options for the step-taking strategy. Two independent runs were carried out for 10^6 basin-hopping steps (minimizations) at a temperature of $k_{\mathrm{B}}T = 0.8\,\mathrm{eV}$; the first starting from known global minimum structures for Gupta potential from the CCD [44], and the second starting from putative global minimum structures for the FS potential for other elements (i.e. starting from Fe for Mo, and vice versa). Runs were continued for a further 10^7 steps if the first two runs did not produce the same prediction for the global minimum.

Each step consisted of a random perturbation to the Cartesian coordinates of every atom in the range `[−max,max]`, where the value of `max` was adjusted every 50 steps to give an average acceptance ratio of 0.5. A suitable initial value for `max` at the chosen temperature is 0.6 Å. A spherical container was used to prevent evaporation during the local minimizations. The convergence parameter for minimization during the basin-hopping runs was taken as $10^{-3}\,\mathrm{eV/\AA}$ for the root mean-square (RMS) gradient, and the lowest 20 minima were converged to an RMS gradient less than $10^{-6}\,\mathrm{eV/\AA}$ at the end of each run.

2.2. *Semi-empirical optimization*

Semi-empirical calculations were carried out using the VAMP software package, which is part of Materials Studio from Accelrys [81]. Geometry optimizations were

Table 3. Value of parameters obtained by least-squares regression fitting to the average energy $E_{avg} = a + bN^{1/3} + cN^{2/3} + dN$ of the FS Fe and Mo global minima plotted in Figure 2.

Parameter	a	b	c	d
Iron	3.452535	-0.81613	2.418055	−4.18369
Molybdenum	13.26858	−13.00072	8.19148	−7.25410

carried out with standard eigenvector-following (EF) optimization techniques [82], with the convergence criterion being a gradient norm of 0.1 kcal mol^{-1} Å^{-1}, using a self-consistent field (SCF) unrestricted Hartree-Fock (UHF) calculation with full Hessian. Each stationary point was verified to be a true minimum by performing a vibrational frequency analysis.

3. Results

We first describe the putative global minima for Fe_N and Mo_N clusters with the FS potential, and then report on their relative stability after further optimization with SE-MO methods.

3.1. *Finnis–Sinclair (FS) putative global minima*

The relative energies, $E(N) - E_{avg}$, of putative global minimum structures for Fe and Mo clusters for N = 3–100 are plotted Figure 2a, together with the second differences, $\Delta_2 E(N) = E(N-1) + E(N+1) - 2E(N)$, between these energies in Figure 2b. In order to remove the effects of increasing cluster size, the absolute cluster energies were reduced by the average energy, E_{avg}, computed from a four-parameter fit to the absolute energies. Parameters for the average energy expression are given for reference in Table 3. A complete set of atomic coordinates and energies for all the suggested global minima will be made available from the Cambridge Cluster Database [44].

It is clear from Figure 2a that the global minima for both Fe and Mo clusters have very similar energies for $N < 26$, but begin to diverge with increasing N. In general, the variation of energy with N is rather smoother in the case of Fe for $N > 50$, indicating that the structures may be less symmetrical than for Mo. However, there are two large coincident troughs in the energy around $N \approx 60$ and $N \approx 80$, which will be described in more detail below. The peaks in $\Delta_2 E(N)$ confirm that there are several magic numbers for stability in the range N = 13–26 for both Fe and Mo but, with increasing N, it appears that Mo clusters are appreciably more stable than Fe for the range of sizes investigated. It was also found that, for $N > 65$, obtaining consistent minimum energy structures for Fe clusters between different basin-hopping optimizations was considerably harder than for Mo clusters of similar size, requiring several independent runs to achieve.

Figure 3 shows the energies of the most stable minima for N = 3–30, together with selected structures. For the majority of clusters with $N < 26$, the geometries and relative energies of the predicted global minima for Fe and Mo clusters are identical. A notable exception is the octahedral cluster $N = 6$ (not shown) which, although isostructural (point group O_h), is higher in energy for Fe than for Mo. For the first two magic numbers, $N = 13$ and $N = 19$, clusters of both Fe and Mo consist of single and double icosahedra, in common with Lennard–Jones (12-6), some Sutton–Chen (12-6, 9-6) and some Gupta (Na, Co) clusters of the same sizes. For the next magic number, $N = 23$, the predicted global minimum structures are again the same for Fe and Mo, but differ from a SC 9-6 cluster of the

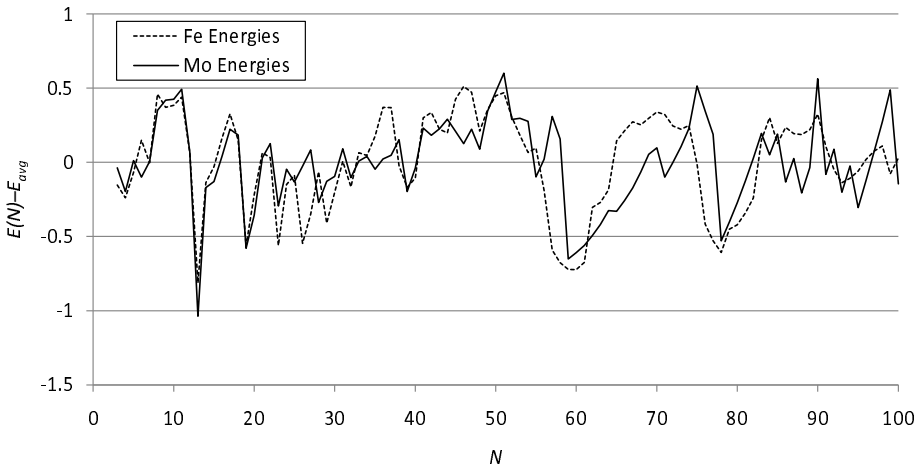

(a)

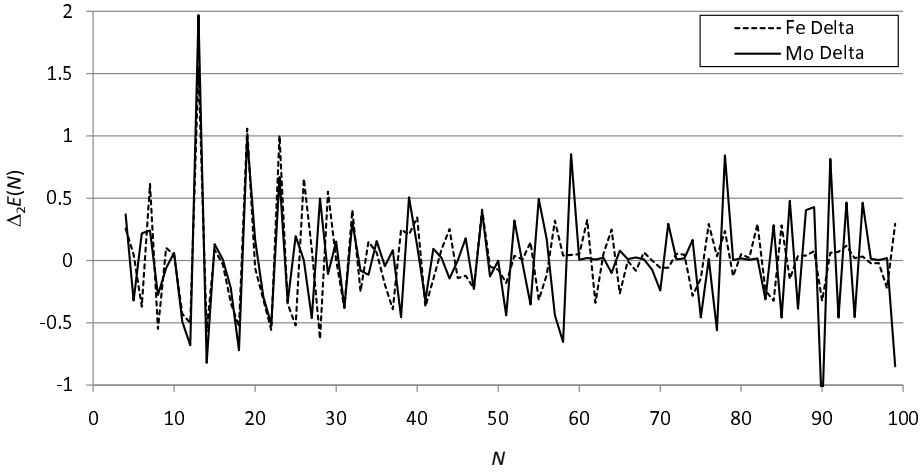

(b)

Figure 2. (a) Energies of putative global minima, $E(N)$, for FS Fe and Mo clusters as a function of size, N, relative to the average energy, E_{avg}, which is defined by $E_{avg} = a+bN^{1/3}+cN^{2/3}+dN$ with the values of parameters a, b, c, d obtained by least-squares regression fitting given in Table 3, and (b) corresponding second differences, $\Delta_2 E(N)$, for the energies in (a).

same size [24], which has point group C_2. Farges et al. [83] first described cluster structures composed of double icosahedra, which they found in rare gas clusters with fewer than 50 atoms [84]. A double icosahedron (DIC) is composed of two interpenetrating 13-atom primitive icosahedra sharing 7 atoms, and contains 19 atoms. Larger polyicosahedral clusters can be made by placing atoms on unoccupied tetrahedral and pentagonal sites; for example $N = 23$, which consists of three interpenetrating DIC with slightly distorted axes. Sakurai et al. have also observed magic number clusters for Fe: $N = 13, 19, 23$ [85, 86] using time-of-flight mass spectrometry, which they attributed to polyicosahedra, and Parks et al. have found further evidence for polyicosahedral structures in ammoniated iron, cobalt and nickel structures [87].

For $N = 26$ and $N = 29$, the global minima for Fe and Mo differ somewhat from previous results for metal clusters, and from each other. Whereas Fe_{26} has point group T_d, consisting of six interpenetrating DIC aligned with their axes approximately parallel to the vertices of an unfilled central tetrahedron, and is relatively stable compared to other Fe clusters of similar size, Mo_{26} is tetragonal (point group C_4) and only of average stability. This result was checked several times by starting optimizations for Fe and Mo clusters from different initial conditions, including

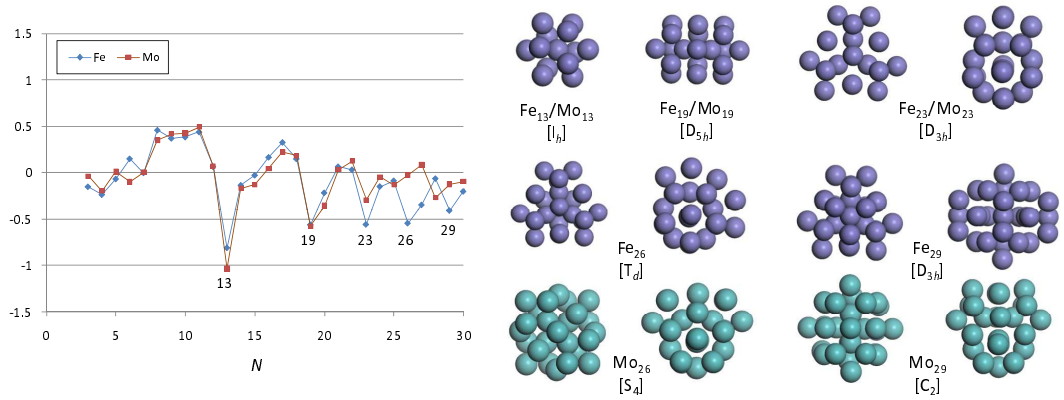

Figure 3. Energies of putative global minima, $E(N)$ for FS Fe and Mo clusters as a function of size, N = 3–30, relative to the average energy, E_{avg}, and (right) corresponding structures for clusters with particularly low energy (point groups are indicated in square brackets).

the global minimum for the other element and, in each case, no other lower energy structures were found. The T_d structure for Fe most resembles those of the LJ 12-6 and Gupta (Co) and Murrell–Mottram (Na) clusters of the same size, but is distinct from SC clusters, which have dihedral or C_s symmetry only. However, the C_4 structure for Mo has no analogue in any metal cluster studied by classical potentials to date, although it is still based on multiple interpenetrating DIC with non-parallel axes. The final magic cluster for $N \leq 30$ is the D_{3h} structure of Fe_{29}, which again resembles that of the LJ 12-6 cluster, whereas Mo_{29} has point group C_2 and more resembles SC 9-6 or 10-8 clusters of the same size. Both are polyicosahedral, with the DIC in Fe_{29} arranged with their axes around a trigonal bipyramidal core, and those in Mo_{29} with their axes approximately at right angles. These results for small clusters demonstrate that the short-range interactions in the FS potential can give rise to structures with a diverse range of optimal geometries. For Fe, the more weakly repulsive nature of the FS potential at short range (see Figure 1a) results in optimal cluster geometries that have higher symmetry compared to the steeper short-range repulsions in Mo clusters.

Moving on to consider larger clusters, Figure 4 shows the energies of the most stable minima for N = 30–60, together with selected structures. From the point of view of comparison with previous metal cluster optimization studies, the most surprising observation for FS potentials is the absence of a stable magic number structure for $N = 38$, which is usually found to be a truncated octahedron (point group O_h) for a very wide range of potentials, including LJ, Gupta, SC, although not MM (Na). Again, this result was checked by starting optimizations for Fe and Mo clusters from different initial conditions, including the O_h structure (which is hard to locate without a transformation of the PES [19, 88]), and found to be robust—it is not simply due to a failure of the basin-hopping algorithm to locate the O_h structure. In fact, in Section 3.2, we show that for Fe_{38}, there is a high symmetry minimum with point group T_h that is even lower-lying than the O_h structure for the FS potential, and which is likely to be the global minimum for PM6. However, for $N = 39$, there do exist stable high symmetry clusters for both Fe and Mo described by the FS potential. Although their structures are markedly different (Fe_{39}, hexagonal, point group C_{6v}; Mo_{39}, pentagonal, point group D_5), their energies relative to the average are approximately equal, indicating that they are very similar in stability. Whereas Fe_{39} consists of 12 interpenetrating DIC, with their axes perpendicular to the six-fold axis, the D_5 structure of Mo_{39} is most unusual, and has no analogue in any metal cluster studied by classical potentials to date. It is based around a distorted central DIC, surrounded by five mutually interpen-

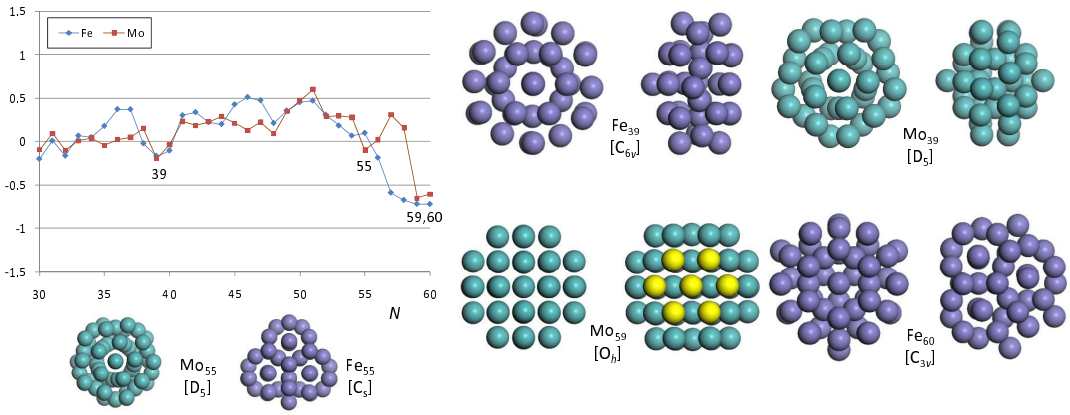

Figure 4. Energies of putative global minima, $E(N)$ for FS Fe and Mo clusters as a function of size, N = 30–60, relative to the average energy, E_{avg}, and (right) corresponding structures for clusters with particularly low energy (with point groups indicated in square brackets). For Mo_{59}, atoms defining a $\{110\}_{bcc}$-type face are highlighted. Fe_{55} and Mo_{55} are also shown, for comparison, despite not being particularly stable.

etrating, partially complete DIC aligned with their axes at approximately 13.8° to the 5-fold axis. Although it is only slightly more stable than average, Mo_{55} bound by a FS potential also has a very similar structure with 5-fold rotational symmetry (point group D_5) in which the surrounding DIC are now complete, whereas all other metal cluster potentials studied to date (with the exception of SC 10-8) predict a very stable Mackay icosahedral (I_h) configuration for $N = 55$. In contrast, FS Fe_{55} is polyicosahedral (C_s) with the DIC axes arranged approximately parallel, and not particularly stable.

At N = 59–60, there is a broad coincident trough in energy for both Fe and Mo clusters, mentioned earlier, which can be seen most clearly in Figure 2a. Although similar in their relative stabilities and high symmetry, the structures of Mo_{59} and Fe_{60} are very different. Whereas Mo_{59} is a complete four-shell bcc particle with octahedral symmetry (point group O_h), Fe_{60} is still polyicosahedral (point group C_{3v}). In Figure 4, the atoms on $\{110\}_{bcc}$-type faces of the O_h structure of Mo_{59} have been highlighted. Although characteristic of bulk crystalline Mo, this structure has not been seen in any finite metal clusters by classical potentials to date. In contrast, the C_{3v} structure of Fe_{60} is trigonal, and more resembles the global optima for SC 9-6 and 10-8 clusters. Its polyicosahedral character is evident when examining the cluster perpendicular to the one of the four three-fold axes and the corresponding mirror plane, and it appears to be built up from interpenetrating DIC arranged around a distorted filled tetrahedral core, with the remaining atoms attached in symmetric positions. The most likely explanation for this difference in structure between clusters of Fe and Mo with $N = 59$ bound by FS potential is again the contrast between short-range repulsions, which allows Fe clusters to adopt a polyicosahedral structure, which maximizes nearest-neighbour packing at the expense of incorporating larger amounts of bulk strain.

Considering the largest group of cluster sizes, Figure 5 shows the energies of the most stable minima found for N = 60–100, together with selected structures. It is clear that for the larger clusters, the variation of the reduced energy, $E(N)$, for $N > 60$ is qualitatively different for the two elements studied, with the curve for Mo showing more precipitous peaks and troughs than for Fe, where the variation is rather smoother. The reason for this behaviour can be seen by contrasting the structures of stable clusters with $N = 78$ for the two elements. Fe_{78} is again polyicosahedral (point group D_{6h}), consisting of six sets of four interpenetrating DIC with their axes, which are slightly distorted, pointing perpendicular to the six-fold

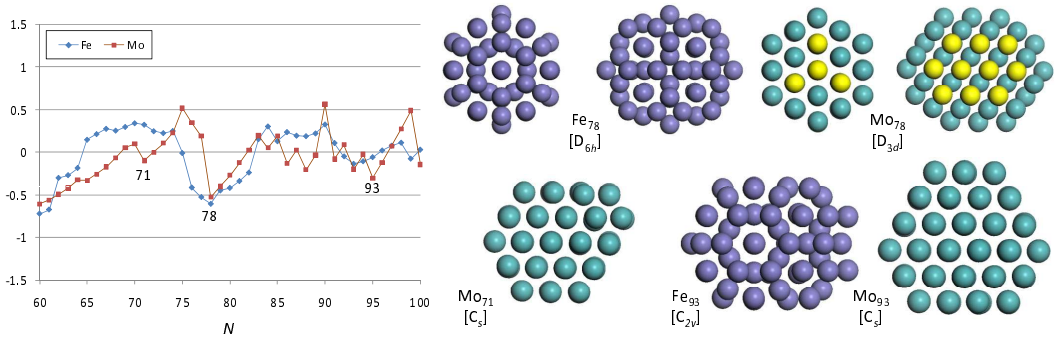

Figure 5. Energies of putative global minima, $E(N)$ for FS Fe and Mo clusters as a function of size, N = 60–100, relative to the average energy, E_{avg}, and corresponding structures (with point groups indicated in square brackets) for clusters with $N = 78$ that are particularly low in energy. For Mo_{78}, atoms defining the three-fold and two-fold axes, respectively, are highlighted. Note that structures with $N = 71$ and 93 are not particularly stable, but are included for comparison.

axis, giving 24 interpenetrating DIC in total. Each set of four DIC has a two-fold axis, which is contained by the mirror plane perpendicular to the six-fold axis, and there are eight additional atoms occupying hexagonal sites surrounding the DIC array. Such a highly symmetrical arrangement is not only relatively stable, but can also accommodate loss or gain of atoms around the DIC array, giving rise to a wide basin of stability around $N = 78$ for Fe clusters. In contrast, Mo_{78} is based around a truncated fragment of a bcc lattice, with a twin plane bisecting the three-fold and two-fold axes (which are highlighted in Figure 4). Similar, but lower symmetry bcc fragments (point group C_s) are also the stable structures found for Mo_{71} and Mo_{93}. In each case, the Mo nanoclusters are truncated by $\{110\}_{bcc}$-type facets. These structures contrast greatly with the behaviour found for Fe, which continues to prefer polyicosahedral structures even for large N, including Fe_{93} (point group C_{2v}) which, although not particularly stable, is shown for comparison with Mo_{93}. Finally, it should be noted that for other types of metal cluster potential, including LJ, Gupta, SC and MM, the stable clusters of size $N = 78$ and 93 have low symmetry (point groups C_s and C_1). Also, for $N = 98$, there is no sign of the Leary tetrahedron [89], which is the most stable structure for the LJ potential, for clusters bound by the FS potential.

For some of the larger iron clusters, the structures can be described in terms of disclinations. A disclination occurs when a nearest-neighbour edge belongs to more (negative disclination) or fewer (positive disclination) than five tetrahedra. Such structures have been analysed in detail for clusters bound by long-ranged Morse potentials, where the global minima were found to have an excess of negative disclinations for values of the Morse range parameter ρ around 3 or less [47, 90]. Polytetrahedral global minima have also been characterised for aluminium clusters [59] bound by a glue model [55], and for binary Lennard-Jones clusters [91] and nanoalloys [63]. The strain associated with polytetrahedral packing in these structures is relieved either by the packing of atoms that have different sizes, or a long range interatomic potential [47, 90, 92–95]. Bulk polytetrahedral crystals, known as Frank-Kasper phases, are found in some alloys [96].

Negative disclinations are evident in the FS global minima of Fe_{55}, Fe_{60}, and Fe_{78}, described above. In each case we relaxed the corresponding structure for the aluminium glue potential [55] and for the Morse potential with $\rho = 3$. We also performed the reverse relaxation from the global minima of the aluminium and Morse clusters using the FS potential for iron. The initial geometries were uniformly scaled before each relaxation according to the mean nearest-neighbour distance. For Fe_{55}, the structure of the corresponding Al_{55} cluster is a low-lying minimum for the

FS potential, and vice versa, but relaxation from the Morse global minimum with $\rho = 3$ involves a significant change in structure. For Fe_{60}, the Morse $\rho = 3$ global minimum and the FS global minimum each relaxed rapidly to a low-lying local minimum with the alternative potential. The aluminium and FS global minima correspond to the same structure. For Fe_{78}, the aluminium global minimum relaxes in a few steps to the previously identified FS global minimum. Conversely, when the FS global minimum was relaxed with the aluminium potential, it produced a structure only of order 10^{-3} eV higher in energy than the aluminium global minimum, with a slight change in radial distances for some atoms.

We then relaxed all the previously reported [59] lowest minima for the aluminium glue potential [55] for the size range $3 \leq N \leq 100$, and in no case was a lower minimum produced. In the size range $3 \leq N \leq 50$ it was found that 34 of the aluminium structures relax to the lowest minimum found with the FS potential, while only six structures are the same for $51 \leq N \leq 100$, and none above $N = 78$. It is likely that the FS global minimum structure corresponds to a low-lying minimum for the aluminium potential for the sizes where the global minima are different. These results clearly illustrate that a 'knowledge-based' approach to global optimization for clusters, where known structures are relaxed with a new potential, can be a very efficient method, although there is the obvious danger of missing a new structural motif.

It is interesting to note that many of the putative global minima we have located display relatively high point group symmetry. This observation provides further support for the predicted correlation between high symmetry and either particularly low or particularly high energy [22, 97, 98]. Furthermore, compared to Fe, the larger Mo_N nanoclusters ($N > 60$) have mainly $\{110\}_{\rm bcc}$ and $\{100\}_{\rm bcc}$-type surface facets, which may be significant in influencing their graphitization ability in carbon nanotube synthesis [99]. However, since the FS potential was originally parameterized for bulk metals, and does not take into account the electronic effects of unfilled d orbitals, we have carried out further optimization of selected global minima described above using SE-MO theory to test the robustness of the structures found.

3.2. *SE-MO optimization from FS global minima*

As demonstrated in a previous study by some of the present authors [100], the use of basin-hopping algorithms using classical potentials to prepare initial structures for further optimization using SE-MO theory is an efficient strategy for exploring the quantum mechanical PES. Despite the approximations made by NDDO methods, such as AM1* and PM6, optimizing the structure of a transition metal cluster with $N \approx 100$ atoms still requires of order several minutes of CPU time, assuming that the starting point is close to an energy minimum (and, if not, the initial self-consistent field calculation will most likely fail to converge), making it impractical at present to carry out basin-hopping directly on the SE-MO PES. In the Conclusions section, we discuss a possible method for overcoming this difficulty, but at this stage we simply note that the putative global minimum energy structures found in the previous Section using the FS potential are easily optimized by AM1* or PM6, and in most cases result in stable structures with similar geometries to classical potential, except for some Jahn-Teller distortion in systems with unfilled d electron shells. However, the relative energies of the SE-MO minima are not always the same as for the FS optimum structures, and in this section we explore this phenomenon by focusing on clusters of size $N = 38$ and $N = 55$. We used both AM1* (for Mo) and PM6 (for Fe) since although the binding energies

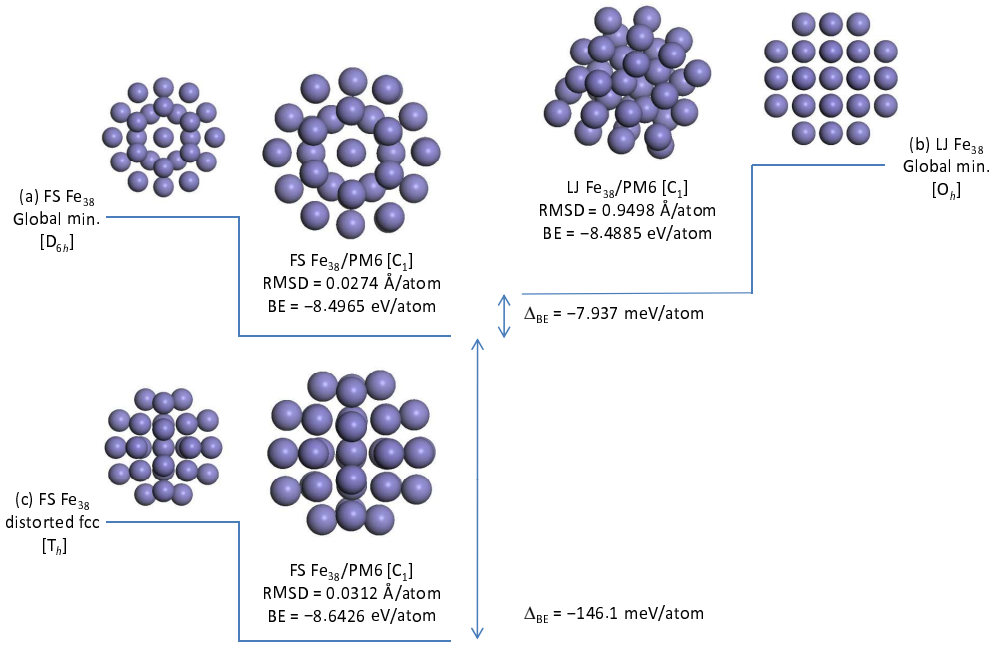

Figure 6. Comparison of relative energies for Fe_{38} clusters after geometry optimization using PM6, starting from three different initial conditions: (a) D_{6h} global minimum for FS Fe_{38} found in Section 3.1, (b) fcc LJ $N = 38$ global minimum scaled for Fe atomic radius, and (c) the T_h (distorted fcc) subsidiary minimum for FS Fe_{38} found during global optimization process. In each case, the new space group, root mean square deviation (RMSD) from initial structure and binding energy (BE) of the new structure are given below it. All energies shown are calculated at the UHF/PM6 level.

of Mo clusters calculated using PM6 agree well with AM1*, their geometries are rather compact and AM1* has been parameterized more extensively for Mo [76] than PM6 [4]. In a previous study by some of the present authors [101], SE-MO results for a Mo_{35} cluster using AM1* were compared directly with DFT using a hybrid exchange functional (B3LYP) and the geometries were found to be in good agreement.

Figure 6 shows the results from a series of geometry optimizations of Fe_{38} clusters using PM6, starting from different initial conditions. The first of these, shown in Figure 6a, is the polyicosahedral FS global minimum for Fe_{38} found in Section 3.1. After optimization with PM6, the geometry of the cluster is only slightly changed (RMSD $= 0.0274$ Å atom^{-1}, although this is sufficient to reduce the point symmetry to C_1), which indicates that the original structure was very close to a minimum on the PM6 PES. Moreover, starting from the fcc LJ global minimum structure for $N = 38$ (actually, a similar structure is metastable for FS Fe_{38} at 3.437 eV above the global minimum), shown in Figure 6b, a heavily distorted (RMSD $= 0.9498$ Å atom^{-1}) low symmetry cluster was obtained in which the atoms are slightly less tightly bound, albeit by only about 8 meV atom^{-1} ($\approx 0.3\,k_{\mathrm{B}}T$ at 298 K). However, a previous study by some of the current authors [100] found that a distorted fcc structure for Mo_{38} is lower in energy than any icosahedral structure at the AM1* level. This might suggest that the final structure in Figure 6a is not the only candidate for the global minimum structure of PM6 Fe_{38}. Indeed, starting from symmetrically distorted (T_h) metastable fcc structure, shown in Figure 6c, which lies 2.682 eV above the global minimum for the FS potential, it was possible to arrive at a structure which is -146.1 meV ($\approx 5.7\,k_{\mathrm{B}}T$ at 298 K) below the original candidate at the PM6 level. Although it is not possible to be certain that this is the global minimum energy structure for PM6 Fe_{38}, we are not aware at this stage of any likely candidates which may lead to lower energy structures. This example also serves as a warning that although the classical PES described by FS potential

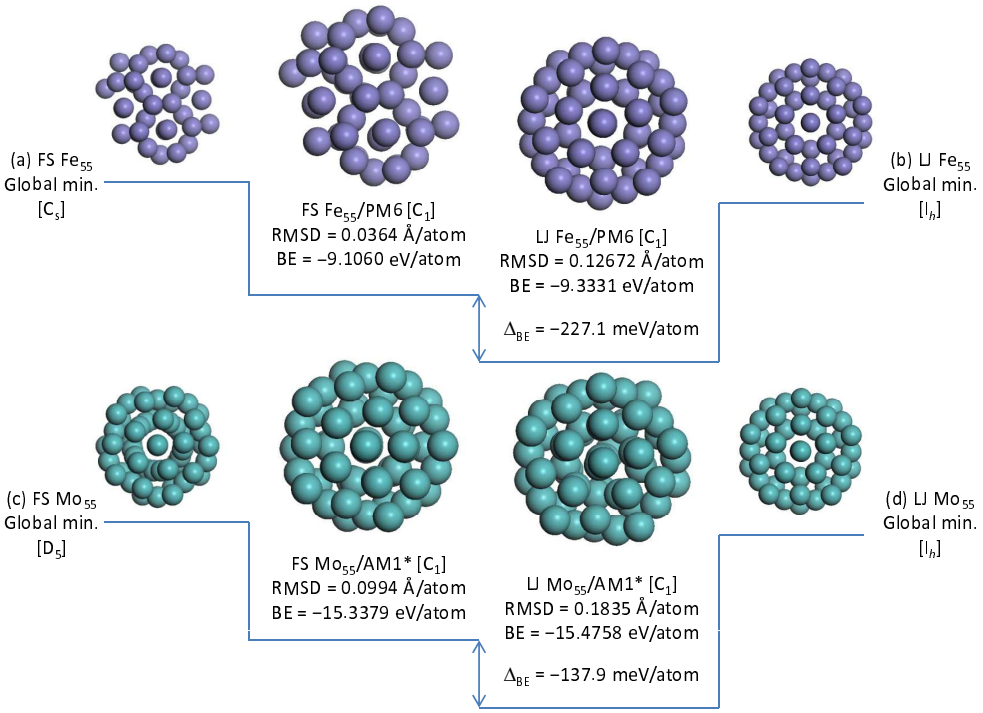

Figure 7. Comparison of relative energies for FS Fe_{55} and Mo_{55} clusters after geometry optimization using PM6, starting from two different initial conditions for each element: (a) C_s global minimum for FS Fe_{55} found in Section 3.1, (b) icosahedral LJ $N = 55$ global minimum scaled for Fe atomic radius, (c) D_s global minimum for FS Mo_{55} found in Section 3.1, and (d) icosahedral LJ $N = 55$ global minimum scaled for Mo atomic radius. In each case, the new space group, root mean square deviation (RMSD) from initial structure and binding energy (BE) of the new structure are given below it. Energies shown are calculated at the UHF/AM1* and UHF/PM6 levels, as indicated.

may be a good guide for initiating a minimization using quantum methods, the relative ordering of minima on these surfaces should not necessarily be expected to agree.

Next, the structures and relative energies for Fe_{55} and Mo_{55} optimized at the AM1* and PM6 levels are compared. In Figure 7a, the polyicosahedral global minimum for Fe_{55} bound by FS potential is optimized via PM6 to a lower symmetry structure which is quite close to the original (RMSD $= 0.0364\,\text{Å}\,\text{atom}^{-1}$). However, in Figure 7b, it can be seen that an equivalent optimization starting from the Mackay icosahedral LJ Fe_{55} global minimum results in a distorted icosahedral cluster (RMSD $= 0.12672\,\text{Å}\,\text{atom}^{-1}$) that is 227.1 meV ($\approx 8.8\,k_\text{B}T$) lower than the one produced from FS global minimum. The situation for Mo_{55} is similar, with the distorted icosahedral structure lying 137.9 meV ($\approx 5.4\,k_\text{B}T$) lower than the distorted D_5 FS global minimum, as shown in Figures 7c and 7d. However, the AM1* optimized FS structure for Mo_{55} has undergone a greater distortion (RMSD $= 0.0994\,\text{Å}\,\text{atom}^{-1}$) and appears to more resemble the distorted icosahedron, thus accounting for the smaller difference in energy of the final structures as compared with Fe_{55}. In a similar fashion, it was also found that the FS potential ranks the low symmetry global minima of Fe/Mo_{75} and Fe/Mo_{98} found in Section 3.1 lower in energy than the decahedral and tetrahedral forms. By contrast, both AM1* and PM6 both rank the distorted high symmetry structures as lower in energy than the FS global minima after SE-MO optimization. These results are all consistent with earlier conclusions of Elliott and Shibuta [100], who found that LJ 12-6 potential generally gives global minimum structures more consistent with SE-MO in comparison with LJ 9-6. This may be an indication that FS and LJ 9-6 have core-core interactions that are too soft, since Fe clusters ($N \leq 32$) studied using DFT [78]

in combination with DFTB showed that Fe_{19} has a non-icosahedral structure as minimum energy [102]. More recent DFT simulations also show that Fe_{55} has an icosahedral structure [103].

4. Conclusions

We have have calculated the putative global minimum energy structures via basin-hopping for Fe and Mo clusters of size $N = 3$–100 atoms bound by Finnis-Sinclair (FS) potentials, and presented a selection of results for the most stable structures along with those corresponding to magic numbers for other types of potential previously used to study metal clusters. Depending on the parameter sets used, the FS potential can give rise to a great diversity of structures; however, for small clusters, these generally consist of different arrangements of interpenetrating double icosahedra (DIC) for both Fe and Mo. As the cluster size increases, Mo clusters tend to adopt a bcc configuration, terminated by {110} and {100}-type facets, whereas Fe clusters continue to take a polyicosahedral form. This difference is caused by the steeper core-core repulsions for FS Mo potential compared to Fe. Whilst there is considerable experimental evidence to support the existence of stable Fe clusters for smaller magic numbers in the polyicosahedral series, there will clearly be a maximum upper limit on the size of such a cluster before it transforms to a more stable structure, e.g. bcc, due to an accumulation of strain energy. Furthermore, SE-MO calculations demonstrate the greater stability of the higher symmetry global minimum structures predicted by pair potentials even for clusters as small as $N = 38, 55, 75$ and 98. Therefore, it would be wise to be cautious in interpreting the global optimum structures predicted by FS potential for transition metal clusters as definitive; "different potentials" lead to "different structures", as found earlier by Doye for lead clusters [45]. However, the FS potential at least provides a reasonable approximation to the semi-empirical quantum mechanical PES, and for this reason it would be valuable in future to carry out basin-hopping with either SE-MO or DFTB using FS potentials as a guiding function to steer the optimization process more efficiently. In addition, a more detailed study of the effects of magnetism on cluster structure is required.

Finally, we would like to briefly remark on the potential relevance of the polyicosahedral clusters found here for Fe clusters in relation to quasicrystals, which have been described as large-scale quasicrystalline cluster aggregates in which the quasilattice is decorated with atomic clusters of the same point group as the quasicrystal [104]. In the same way that the polytetrahedral clusters studied by Doye and Wales [90] may form building blocks of crystalline Frank-Kasper phases or quasicrystals with tetrahedral point groups, the polyicosahedral structures found here may play a role in quasicrystals with multishell icosahedral clusters or metallic glasses composed of primitive icosahedral aggregates.

Acknowledgements

J.A.E. gratefully acknowledges Japan Society for Promotion of Science (JSPS) for funding of a Long Term Invitation Fellowship (No. L08536), held at the University of Tokyo, and both authors would like to thank Fitzwilliam College, Cambridge for supporting a visiting Fellowship for Y.S. Part of this research was supported by the Grant-in-Aid for Young Scientists (a) (No. 18686017) from MEXT, Japan. The authors wish to acknowledge helpful discussions with Prof. Eiji Abe of University of Tokyo.

References

[1] M.W. Finnis and J.E. Sinclair, Phil. Mag. A 50 (1984) p.45–55.
[2] M.W. Finnis and J.E. Sinclair, Phil. Mag. A 53 (1986) p.161.
[3] P. Winget, C. Selcuki, A.H.C. Horn, B. Martin and T. Clark, Theoretical Chemistry Accounts 110 (2003) p.254–266.
[4] J.J.P. Stewart, Journal of Molecular Modeling 13 (2007) p.1173–1213.
[5] P. Entel, M.E. Gruner, G. Rollmann, A. Hucht, S. Sahoo, A.T. Zayak, H.C. Herper and A. Dannenberg, Phil. Mag. 88 (2008) p.2725–2738.
[6] H. Dai, A. Rinzler, P. Nikolaev, A. Thess, D.T. Colbert and R.E. Smalley, Chem. Phys. Lett. 260 (1996) p.471–475.
[7] S. Maruyama, R. Kojima, Y. Miyauchi, S. Chiashi and M. Kohno, Chem. Phys. Letters 360 (2002) p.229–234.
[8] Y.L. Li, I.A. Kinloch and A.H. Windle, Science 304 (2004) p.276–278.
[9] J.A. Elliott, M. Hamm and Y. Shibuta, J. Chem. Phys. 130 (2009) 034704.
[10] R.S. Berry and D.J. Wales, Phys. Rev. Lett. 63 (1989) p.1156–1159.
[11] D.J. Wales and R.S. Berry, J. Chem. Phys. 92 (1990) p.4473–4482.
[12] Y. Shibuta and T. Suzuki, Chem. Phys. Letters 445 (2007) p.265–270.
[13] I.M.L. Billas, A. Chatelain and W.A. deHeer, J. Magn. Magn. Mater. 168 (1997) p.64–84.
[14] F.H. Stillinger and T.A. Weber, Science 225 (1984) p.983.
[15] D.J. Wales and J.P.K. Doye, J. Chem. Phys. 119 (2003) p.12409–12416.
[16] D.J. Wales and H.A. Scheraga, Science 285 (1999) p.1368–1372.
[17] D.J. Wales and T.V. Bogdan, J. Phys. Chem. B 110 (2006) p.20765–20776.
[18] M.A. Miller, J.P.K. Doye and D.J. Wales, J. Chem. Phys. 110 (1999) p.328–334.
[19] J.P.K. Doye, M.A. Miller and D.J. Wales, J. Chem. Phys. 110 (1999) p.6896–6906.
[20] J.P. Neirotti, F. Calvo, D.L. Freeman and J.D. Doll, J. Chem. Phys. 112 (2000) p.10340–10349.
[21] F. Calvo, J.P. Neirotti, D.L. Freeman and J.D. Doll, J. Chem. Phys. 112 (2000) p.10350–10357.
[22] D.J. Wales *Energy Landscapes*, Cambridge University Press, Cambridge, 2003.
[23] D.J. Wales and J.P.K. Doye, J. Phys. Chem. A 101 (1997) p.5111–5116.
[24] J.P.K. Doye and D.J. Wales, New J. Chem. 22 (1998) p.733–744.
[25] Z.Q. Li and H.A. Scheraga, Proc. Natl. Acad. Sci. USA 84 (1987) p.6611–6615.
[26] D.M. Deaven and K.M. Ho, Phys. Rev. Lett. 75 (1995) p.288–291.
[27] D.M. Deaven, N. Tit, J.R. Morris and K.M. Ho, Chem. Phys. Letters 256 (1996) p.195–200.
[28] G.W. Turner, E. Tedesco, K.D.M. Harris, R.L. Johnston and B.M. Kariuki, Chem. Phys. Lett. 321 (2000) p.183–190.
[29] D.J. Wales and M.P. Hodges, Chem. Phys. Lett. 286 (1998) p.65–72.
[30] M.P. Hodges and D.J. Wales, Chem. Phys. Lett. 324 (2000) p.279–288.
[31] P. Derreumaux, J. Chem. Phys. 106 (1997) p.5260–5270.
[32] P. Derreumaux, J. Chem. Phys. 107 (1997) p.1941–1947.
[33] M.A. Miller and D.J. Wales, J. Chem. Phys. 111 (1999) p.6610–6616.
[34] P.N. Mortenson and D.J. Wales, J. Chem. Phys. 114 (2001) p.6443–6454.
[35] P.N. Mortenson, D.A. Evans and D.J. Wales, J. Chem. Phys. 117 (2002) p.1363–1376.
[36] J.M. Carr and D.J. Wales, J. Chem. Phys. 123 (2005) 234901.
[37] A. Verma, A. Schug, K.H. Lee and W. Wenzel, J. Chem. Phys. 124 (2006) 044515.
[38] F. Calvo, J.P.K. Doye and D.J. Wales, J. Chem. Phys. 116 (2002) p.2642–2649.
[39] T.F. Middleton, J. Hernández-Rojas, P.N. Mortenson and D.J. Wales, Phys. Rev. B 64 (2001) 184201.
[40] S.N. Fejer and D.J. Wales, Phys. Rev. Lett. 99 (2007) 086106.
[41] S. Fejer, T. James, J. Hernandez-Rojas and D. Wales, Phys. Chem. Chem. Phys. 11 (2009) p.2098–2104.
[42] D.J. Wales, GMIN: A program for basin-hopping global optimisation and basin-sampling thermodynamics; .
[43] D. Cvijovic and J. Klinowski, Science 267 (1995) p.664–666.
[44] D.J. Wales, J.P.K. Doye, A. Dullweber, M.P. Hodges, F. Naumkin, F. Calvo, J. Hernández-Rojas and T.F. Middleton, The Cambridge Cluster Database; .
[45] J.P.K. Doye, Comp. Mater. Sci. 35 (2006) p.227–231.
[46] A.P. Sutton and J. Chen, Phil. Mag. Lett. 61 (1990) p.139–146.
[47] J.P.K. Doye and D.J. Wales, J. Chem. Soc. : Farad. Trans. 93 (1997) p.4233–4243.
[48] E.G. Noya, J.P.K. Doye, D.J. Wales and A. Aguado, Eur. Phys. J. D 43 (2007) p.57–60.
[49] R.P. Gupta, Phys. Rev. B 23 (1981) p.6265–6270.
[50] Y. Li, E. Blaisten-Barojas and D. Papaconstantopoulos, Phys. Rev. B 57 (1998) p.15519–15532.
[51] J.N. Murrell and R.E. Mottram, Mol. Phys. 69 (1990) p.571–585.
[52] J.Y. Fang, R.L. Johnston and J.N. Murrell, Mol. Phys. 78 (1993) p.1405–1422.
[53] H. Cox, R.L. Johnston and J.M. Murrell, J. Solid Stat. Chem. 145 (1999) p.517–540.
[54] E.G. Noya, J.P.K. Doye and F. Calvo, Phys. Rev. B 73 (2006) 125407.
[55] F. Ercolessi and J.B. Adams, Europhys. Lett. 26 (1994) p.583–588.
[56] J.P.K. Doye and S.C. Hendy, Eur. Phys. J. D 22 (2003) p.99–107.
[57] H.S. Lim, C.K. Ong and F. Ercolessi, Surf. Sci. 269/270 (1992) p.1109–1115.
[58] E.M. Fernández, J.M. Soler, I.L. Garzón and L.C. Balbś, Phys. Rev. B 70 (2004) 165403.
[59] J.P.K. Doye, Phys. Rev. B 68 (2003) 195418.
[60] L. Zhan, J.Z.Y. Chen, W.K. Liu and S.K. Lai, J. Chem. Phys. 122 (2005) 244707.
[61] Z.Y. Li, N.P. Young, M. Di Vece, S. Palomba, R.E. Palmer, A.L. Bleloch, B.C. Curley, R.L. Johnston, J. Jiang and J. Yuan, Nature 451 (2008) p.46–48.
[62] D. Parodi and R. Ferrando, Phys. Lett. A 367 (2007) p.215–219.
[63] R. Ferrando, J. Jellinek and R.L. Johnston, Chem. Rev. 108 (2008) p.845–910.
[64] W.H. Chiang and R.M. Sankaran, Adv. Mater. 20 (2008) p.4857–+.

[65] M.S. Motta, A. Moisala, I.A. Kinloch and A.H. Windle, Journal of Nanoscience and Nanotechnology 8 (2008) p.2442–2449.
[66] C. Kittel *Introduction to Solid State Physics*, 7th ed. Wiley, New York, 1996.
[67] J.P. Hirth and J. Lothe *Theory of dislocations*, 2nd ed. Wiley, New York, 1982.
[68] G.Y. Guo and H.H. Wang, Chin. J. Phys. 38 (2000) p.949–961.
[69] L. Marville and W. Andreoni, J. Phys. Chem. 91 (1987) p.2645–2649.
[70] Y. Shibuta and T. Suzuki, J. Chem. Phys. 129 (2008) 144102.
[71] N.A. Besley, R.L. Johnston, A.J. Stace and J. Uppenbrink, J. Molec. Struct. - Theochem 341 (1995) p.75–90.
[72] D. Tománek, S. Mukherjee and K.H. Bennemann, Phys. Rev. B 28 (1983) p.665–673.
[73] J.N. Murrell, J. Molec. Struct. - Theochem 424 (1998) p.93–99.
[74] T. Bredow and K. Jug, Theor. Chem. Acc. 113 (2005) p.1–14.
[75] M.J.S. Dewar, E.G. Zoebisch, E.F. Healy and J.J.P. Stewart, J. Am. Chem. Soc. 107 (1985) p.3902–3909.
[76] A.A. Voityuk and N. Rösch, J. Phys. Chem. A 104 (2000) p.4089–4094.
[77] W. Thiel and A.A. Voityuk, Theoret. Chim. Acta 81 (1992) p.391–404.
[78] C. Köhler, G. Seifert and T. Frauenheim, Chem. Phys. 309 (2005) p.23–31.
[79] A. Leach *Molecular modelling: principles and applications*, 2nd ed. Pearson Education Ltd., Harlow, 2001.
[80] A. Morrish *The physical principles of magnetism*, John Wiley, New York, 1965.
[81] Materials Studio Modeling Environment v. 4.4; .
[82] J. Baker, J. Comp. Chem. 7 (1986) p.385–395.
[83] J. Farges, M.F. Deferaudy, B. Raoult and G. Torchet, Surf. Sci. 156 (1985) p.370–378.
[84] J. Farges, M.F. Deferaudy, B. Raoult and G. Torchet, J. Chem. Phys. 78 (1983) p.5067–5080.
[85] M. Sakurai, K. Watanabe, K. Sumiyama and K. Suzuki, J. Phys. Soc. Japan 67 (1998) p.2571–2573.
[86] M. Sakurai, K. Watanabe, K. Sumiyama and K. Suzuki, J. Chem. Phys. 111 (1999) p.235–238.
[87] E.K. Parks, B.J. Winter, T.D. Klots and S.J. Riley, J. Chem. Phys. 96 (1992) p.8267–8274.
[88] J.P.K. Doye, D.J. Wales and M.A. Miller, J. Chem. Phys. 109 (1998) p.8143–8153.
[89] R.H. Leary and J.P.K. Doye, Phys. Rev. E 60 (1999) R6320-R6322.
[90] J.P.K. Doye and D.J. Wales, Phys. Rev. Lett. 86 (2001) p.5719–5722.
[91] J.P.K. Doye and L. Meyer, Phys. Rev. Lett. 95 (2003) p.063401.
[92] P.A. Braier, R.S. Berry and D.J. Wales, J. Chem. Phys. 93 (1990) p.8745–8756.
[93] J.P.K. Doye, D.J. Wales and R.S. Berry, J. Chem. Phys. 103 (1995) p.4234–4249.
[94] J.P.K. Doye and D.J. Wales, J. Phys. B 29 (1996) p.4859–4894.
[95] J.P.K. Doye and D.J. Wales, Science 271 (1996) p.484–487.
[96] F.C. Frank and J.S. Kasper, Acta Cryst. 11 (1958) p.184.
[97] D.J. Wales, Chem. Phys. Lett. 285 (1998) p.330–336.
[98] D.J. Wales, Chem. Phys. Lett. 294 (1998) p.262.
[99] Y. Shibuta and J.A. Elliott, Chem. Phys. Lett. 472 (2009) p.200–206.
[100] J.A. Elliott and Y. Shibuta, J. Comput. Theor. Nanosci. 6 (2009) p.1443–1451.
[101] J.A. Elliott and Y. Shibuta, Mol. Sim. 34 (2008) p.891–903.
[102] P. Bobadova-Parvanova, K.A. Jackson, S. Srinivas, M. Horoi, C. Köhler and G. Seifert, J. Chem. Phys. 116 (2002) p.3576–3587.
[103] G. Rollmann, M.E. Gruner, A. Hucht, R. Meyer, P. Entel, M.L. Tiago and J.R. Chelikowsky, Phys. Rev. Lett. 99 (2007) 083402.
[104] E. Abe, Y. Yan and S.J. Pennycook, Nature Materials 3 (2004) p.759–767.